AIP | Review of Scientific Instruments

Two-dimensional diagnostic of edge plasma structure using a lithium beam probe in a compact helical system

K. Nakamura, H. Iguchi, M. Ueda, Z. Narihiro, A. Shimizu, T. Morisaki, M. Isobe, C. Takahashi, S. Nishimura, C. Suzuki, Y. Yoshimura, K. Nagaoka, T. Minami, M. Yoshinuma, K. Ida, S. Okamura, and K. Matsuoka

Citation: Review of Scientific Instruments **76**, 013504 (2005); doi: 10.1063/1.1809284
View online: http://dx.doi.org/10.1063/1.1809284
View Table of Contents: http://scitation.aip.org/content/aip/journal/rsi/76/1?ver=pdfcov
Published by the AIP Publishing

Two-dimensional diagnostic of edge plasma structure using a lithium beam probe in a compact helical system

K. Nakamura[a)]
The Graduate University for Advanced Studies, 322-6 Oroshi-Cho, Toki 509-5292, Japan

H. Iguchi
National Institute for Fusion Science, Toki 509-5292, Japan

M. Ueda
National Institute for Space Research, Sao Jose dos Campos, SP, Brazil

Z. Narihiro
Nagoya University, Nagoya 462-8601, Japan

A. Shimizu, T. Morisaki, M. Isobe, C. Takahashi, S. Nishimura, C. Suzuki, Y. Yoshimura, K. Nagaoka, T. Minami, M. Yoshinuma, K. Ida, S. Okamura, and K. Matsuoka
National Institute for Fusion Science, Toki 509-5292, Japan

(Received 23 October 2003; accepted 24 June 2004; published online 22 December 2004)

A neutral lithium beam probe for two-dimensional diagnosis of edge plasmas has been designed and installed on the compact helical system. A lithium beam with an energy of 15 keV and a current of 0.1 mA is used. The spatial resolution is about 10 mm, and the time response is about 10 ms. The beam penetration depth is expressed in terms of the line integral density $\langle n_e l \rangle$, which is about 2×10^{18} m^{-2}. The beam injection angle can be varied and the observation point covers the edge and separatrix region of the helical diverter configuration. Two-dimensional electron density profiles for electron cyclotron heating and neutral beam injection (NBI) heated plasmas are obtained near and outside the last closed flux surface (LCFS). Analysis for two-dimensional density profile reconstruction indicates that significant amounts of surface plasma are confined outside the LCFS for NBI plasmas even though the ergodic layer is cut by the vacuum chamber wall (inboard limiter configuration). The usefullness of this new two-dimensional diagnostic in the edge region is demonstrated. © *2005 American Institute of Physics.* [DOI: 10.1063/1.1809284]

I. INTRODUCTION

The determination of plasma parameters in the edge region of magnetically confined plasmas has become an important issue because plasma properties in the region have a key role in determining the global plasma confinement. Understanding and controlling edge plasmas are also important from the point of view of the divertor design for fusion reactors. In nonaxisymmetric helical devices, edge magnetic configurations intrinsically include ergodic layer and magnetic island structures. A helical device like the large helical device (LHD) or the compact helical system (CHS) has a toroidally continuous natural divertor similar to double-null X point structure in tokamaks. However the magnetic lines of force in this region have a chaotic behavior forming an ergodic region. The separatrix is not as clear as that in tokamaks. The roles of the ergodic layer such as the screening of impurities and the fueling of neutral particles have been discussed, but no clear physical picture has been obtained. It is important to measure the plasma distribution and its parameters in this layer.

Measurement of plasma density in the separatrix region is also important from the diagnostic point of view. The core plasma density profile is often determined by Abel inversion of multichannel interferometers. In the case of a heliotron-type device, the chord inevitably passes the separatrix region. Ambiguity of the electron density in this region affects the accuracy of the core density profile determination. In order to study the plasma structure in this area, two-dimensional measurements are essential.

A lithium beam probe (LiBP) is one of the best techniques for the measurement of the edge plasma density profile. This method, which utilizes the emission of the injected neutral lithium beam by electron impact excitation was developed by Kadota *et al.*[1] The LiBP can probe plasmas from the edge to the core crossing the last closed flux surface (LCFS) without perturbation or contamination of the plasma. It has been used in many magnetic confinement devices such as NBT-1M,[2] ASDEX,[3] TEXTOR,[4] CHS,[5] WVII-AS,[6] JET,[7] TEXT,[8] DIII-D,[9] and more recently LHD.[10] But all those measurements are in one dimension along a fixed beam line.

A LiBP system that can measure two-dimensional plasma structure in the edge plasma region including the separatrix has been designed and installed on CHS. This system has a beam injector with variable injection angle and a multichannel optical detection system. Changing the beam injection angle shot by shot, a two-dimensional beam emis-

[a)]Electronic mail: nkiichi@nifs.ac.jp

sion profile is obtained. Taking the related atomic processes into account, the emission profile is converted to the electron density profile.

II. BRIEF DESCRIPTION OF LiBP SPECTROSCOPY

Lithium atoms injected into plasmas are excited by collisions with plasma particles and emit photons in a series of spectral lines. The intensity of LiI resonance line ($2p$-$2s$/670.8 nm) is the strongest one among them. Let us consider the situation of detecting those photons with an optical system of solid angle Ω, sampling volume V, and efficiency, η. The number of photons $N_{vp}(x)$ to be detected is described as

$$N_{vp}(x) = n_e(x) n_b(x) \langle \sigma_{\mathrm{em}} v_r \rangle_{\mathrm{eff}} \Omega / 4\pi V \eta, \tag{1}$$

where, $n_e(x)$ is the electron density, $n_b(x)$ is the lithium atom density, $\langle \sigma_{\mathrm{em}} v \rangle_{\mathrm{eff}}$ is the effective emission rate coefficient of the resonance line, and x is the distance along the beam. Here v_r is the relative velocity between plasma particles and the lithium atom.

The number of lithium atoms at the $2p$ state, $n_{\mathrm{Li}\text{-}p}$, which is the emission source of the resonance line, is primary determined by the balance between excitation from the ground state and spontaneous emission (the life time τ_{em} of 27 ns.) However, multiple loss processes such as ionization, charge exchange, excitation to upper levels, etc., also contribute to its dependence on the electron density. The effective emission rate coefficient $\langle \sigma_{\mathrm{em}} v_r \rangle_{\mathrm{eff}}$ is defined as follows:[5]

$$\frac{n_{\mathrm{Li}-p}}{\tau_{\mathrm{em}}} = n_e \langle \sigma_{\mathrm{em}} v_r \rangle_{\mathrm{eff}} n_b. \tag{2}$$

It is related with the plasma particles impact excitation rate coefficient from the $2s$ to $2p$ state as

$$\langle \sigma_{\mathrm{em}} v_r \rangle_{\mathrm{eff}} = \frac{\langle \sigma_{ex} v_r \rangle}{1 + n_e \{ \langle \sigma_{\mathrm{dex}} v_r \rangle + \langle \sigma_{\mathrm{ip}} v_r \rangle + \langle \sigma_{\mathrm{ex}} v_r \rangle \} \tau_{\mathrm{em}}}. \tag{3}$$

Here, $\langle \sigma_{\mathrm{ex}} v_r \rangle$, $\langle \sigma_{\mathrm{dex}} v_r \rangle$ and $\langle \sigma_{\mathrm{ip}} v_r \rangle$ are the rate coefficient of excitation, deexcitation, and ionization from the $2p$ state, respectively. These rate coefficients include the effects from the electron and the ion. For example, the excitation rate coefficient is defined as follows:

$$\langle \sigma_{\mathrm{ex}} v_r \rangle = \langle \sigma_{\mathrm{ex}} v_{r-e} \rangle + \langle \sigma_{\mathrm{ex}} v_{r-i} \rangle, \tag{4}$$

where $\langle \sigma_{\mathrm{ex}} v_{r-e} \rangle$ is the electron impact excitation rate coefficient, and $\langle \sigma_{\mathrm{ex}} y_{r-i} \rangle$ is the ion impact excitation rate coefficient. Here, v_{r-e} is the relative electron velocity and v_{r-i} is the relative ion velocity with respect to the lithium beam.

In general, the LiBP is used for edge plasmas where electron and ion temperatures are less than a few hundred electron volts. Since the temperature dependence of the rate coefficient for electron impact excitation is very weak in the range from 10 eV to a few hundred electron volts, it is usually assumed to be constant. Of course, this assumption is broken when electron temperature becomes less than 10 eV. The rate coefficient for the ion impact excitation is also constant because relative velocity is determined by the lithium beam velocity in this temperature range. The effective emission rate coefficient described in Eq. (3) includes both contributions. The beam density is also a function of the location in the plasma, because it suffers attenuation due to ionization and charge exchange processes. Then the unknown parameters in Eq. (1) are $n_e(x)$ and $n_b(x)$. Equation (1) is rewritten as follows:

$$n_e(x) = \frac{N_{vp}(x)}{n_b(x) \langle \sigma_{\mathrm{em}} v_r \rangle_{\mathrm{eff}} \Omega / 4\pi V \eta}. \tag{5}$$

In the region that the plasma density is small and the beam attenuation is negligible, the beam emission intensity is proportional to the electron density. In this case, Eq. (5) can simply be written as

$$n_e(x) = \frac{N_{vp}(x)}{n_b(0) \langle \sigma_{\mathrm{em}} v_r \rangle_{\mathrm{eff}} \Omega / 4\pi V \eta} = \frac{\alpha}{\langle \sigma_{\mathrm{em}} v_r \rangle_{\mathrm{eff}}} N_{vp}(x). \tag{6}$$

Here $\alpha = 1/n_b(0)\Omega/4\pi V\eta$ is a proportional constant. Then the electron density profile simply coincides with the beam emission profile.

When the beam attenuation is not negligible, which is usually the case, there are two methods to convert the beam emission profile to the electron density profile. The first one is the beam attenuation method and the other is the beam intensity method.

A. Beam attenuation method

When the beam is fully attenuated within the observation area, the beam attenuation method can be used. Electron density $n_e(x)$ is determined by integrating the $N_{vp}(x)$ from the position x toward the emission tail-off position x_1.

Beam attenuation due to ionization is expressed as

$$\frac{1}{n_b(x)} \frac{\mathrm{d}n_b(x)}{\mathrm{d}x} = -n_e(x) \frac{\langle \sigma_{\mathrm{ion}} v_r \rangle_{\mathrm{eff}}}{v_b}, \tag{7}$$

where $\langle \sigma_{\mathrm{ion}} v \rangle_{\mathrm{eff}}$ is the effective ionization rate coefficient and v_b is the lithium beam velocity. Then the beam density is described as

$$n_b(x) = n_{b0} \exp\left(- \int_0^x n_e(l) \frac{\langle \sigma_{\mathrm{ion}} v_r \rangle_{\mathrm{eff}}}{v_b} \mathrm{d}l \right). \tag{8}$$

Solving for $n_e(x)$ in Eq. (1), and substituting it into Eq. (8), finally integrating from x to x_1, the beam density $n_b(x)$ is alternatively expressed as

$$\begin{aligned} n_b(x) &= - \int_x^{x_1} \frac{\mathrm{d}n_b(l)}{\mathrm{d}l} \mathrm{d}l \\ &= \int_x^{x_1} \left[N_{vp}(l) \frac{\langle \sigma_{\mathrm{ion}} v_r \rangle_{\mathrm{eff}}}{\langle \sigma_{\mathrm{em}} v_r \rangle_{\mathrm{eff}}} \Big/ (\Omega/4\pi) V \eta v_b \right] \mathrm{d}l. \end{aligned} \tag{9}$$

Combining Eqs. (1) and (9), the electron density now can be expressed as

$$n_e(x) = \frac{N_{vp}(x) v_b}{\langle \sigma_{\mathrm{em}} v_r \rangle_{\mathrm{eff}}} \Big/ \int_x^{x_1} N_{vp}(l) \frac{\langle \sigma_{\mathrm{ion}} v_r \rangle_{\mathrm{eff}}}{\langle \sigma_{\mathrm{em}} v_r \rangle_{\mathrm{eff}}} \mathrm{d}l. \tag{10}$$

Now the electron density profile is determined by the ratio of the local beam emission intensity and its integration

from the emission tail-off position (beam attenuation position) to the observation point. No calibration is necessary, which is the advantage of this method.

Since the ratio $\langle\sigma_{\mathrm{ion}}v_r\rangle_{\mathrm{eff}}/\langle\sigma_{\mathrm{em}}v_r\rangle_{\mathrm{eff}}$ is a function of the electron density, an iteration process is necessary to obtain the electron density profile. Assuming the ratio at the low density limit to be constant and giving it as an initial value, the initial density profile for iteration can simply be obtained as

$$n_e(x) = \frac{N_{vp}(x)v_b}{\langle\sigma_{\mathrm{ion}}v_r\rangle_{\mathrm{eff}}} \Bigg/ \int_x^{x_1} N_{vp}(l)\mathrm{d}l. \tag{11}$$

Then the final density profile is calculated from Eq. (10) by iteration.

B. Beam intensity method

The other method is the beam intensity method, which can be used when the beam is not fully attenuated within the observation area. The electron density $n_e(x)$ is derived from the beam emission intensity $N_{vp}(x)$ based on the atomic data, sensitivity of the optical system and the beam density $n_b(x)$.

For a given density profile initially, the emission intensity $N_{vp}(x)$ can be calculated numerically using Eqs. (1) and (8), which is denoted as $N^*_{vp}(x)$ here. It is written in terms of the constant α defined in Eq. (6) as

$$N^*_{vp}(x) = n_e(x)\frac{\langle\sigma_{\mathrm{em}}v_r\rangle_{\mathrm{eff}}}{\alpha}\exp\left(-\int_0^x n_e(l)\frac{\langle\sigma_{\mathrm{ion}}v_r\rangle_{\mathrm{eff}}}{v_b}\mathrm{d}l\right). \tag{12}$$

The electron density is determined by iteration so that the observed emission intensity $N_{vp}(x)$ coincides with the numerically calculated $N^*_{vp}(x)$.

In general, the constant α can be determined by a calibration method using a gas target. A lithium beam is injected into a uniform gas target with known pressure and emission is detected with the same optical system. In this case absolute values of the collisional excitation cross section and number density of the target gas have to be given.[1] Alternatively the α can be given experimentally using the beam a attenuation method, which method is adopted in this article and will be described in Sec. V.

III. EDGE MAGNETIC FIELD STRUCTURE IN CHS

CHS is a low aspect ratio helical device with a major radius of 1.0 m and an average minor radius of 0.2 m. The pole number and the toroidal period of the helical field coils are $l=2$ and $m=8$, respectively. The toroidal ripple in magnetic field strength ε_t is about 0.2 and is comparable to the helical ripple ε_h near the plasma edge. In CHS, a variety of edge magnetic field configurations can be realized by changing the position of the magnetic axis.

The field line structures in the edge region are calculated for two typical magnetic configurations, namely, the inboard limiter case and the magnetic limiter case. Each configuration is realized by an inward-shifted or outward-shifted magnetic axis, respectively. Poincare plots of the magnetic field lines on a poloidal cross section outside the LCFS for $R_{\mathrm{ax}}=0.921$ m and $R_{\mathrm{ax}}=0.995$ m are shown in Figs. 1(a) and 1(b). It is noted that the starting points of the field line trace are uniformly distributed outside the LCFS and the plotted points are the superposition of the points on a poloidal cross section at every 45° in toroidal direction reflecting the m number of 8. The field line trace is terminated if it crosses the vacuum chamber wall. These figures qualitatively provide the image of the field line ergodicity outside the LCFS, although it is not a direct indication of the field line connection length to the wall.

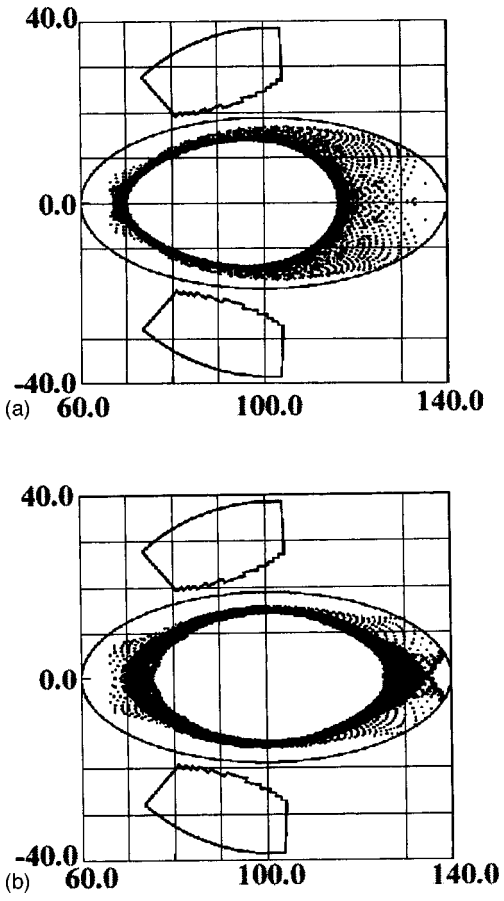

FIG. 1. Poincare plots of the magnetic field line on a poloidal cross section (every 45° in toroidal direction) outside the LCFS for (a) $R_{\mathrm{ax}}=0.921$ m and (b) $R_{\mathrm{ax}}=0.995$ m.

The normal operational configuration in CHS is the inward-shifted configuration at $R_{\mathrm{ax}}=0.921$ m, in which the plasma performance is generally maximized. In this case the inboard walls at eight positions in the toroidal direction play a role of material limiter. The ergodic layer disappears, which is in contrast to the magnetic limiter configuration.

IV. EXPERIMENTAL SETUP

The two-dimensional (2D)-LiBP system has been installed on the CHS as shown in Fig. 2. The coordinate system used here is defined as follows. The x axis is taken as the same as the major radius on the equatorial plane measured from the toroidal axis y. The x-y plane is defined at the poloidal cross section where the beam injection and detection optics are located.

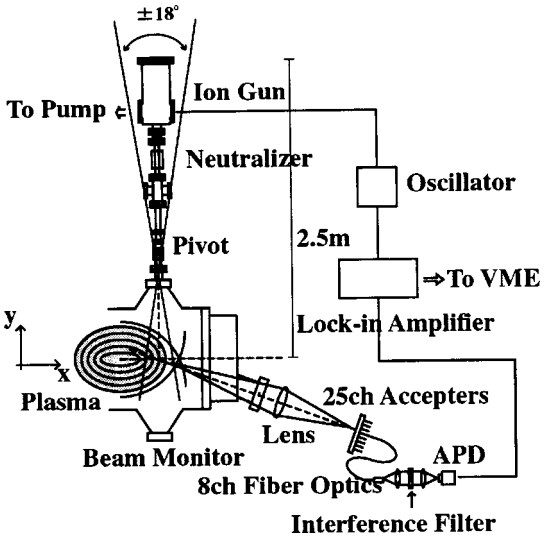

FIG. 2. Experimental setup for the 2D-LiBP system on CHS. Two-dimensional profile is obtained by changing the beam injection angle shot by shot.

The system consists of two parts. One is a beam injection system that generates and injects the neutral Li beam. The other is an optical detection system that observes light emission from the injected Li beam by the collision with plasma particles.

The Li-beam injector is located on the upper side of the torus. The injector consists of an ion gun with a Li source (6 mm diameter) which is thermoionic emission-type β-eucryptite, with a Pierce extractor and a cylindrical lens. This section is covered with a magnetic shield in order to prevent the effect of the CHS stray field. Figure 3 shows a schematic drawing of the beam gun. The Li beam is extracted from the source and accelerated and focused by the Pierce gun and cylindrical lens. The beam energy is in the range from 10 to 20 keV with an equivalent neutral beam current of about 0.1 mA. The ion beam is neutralized in the Cs neutralizing cell. Figure 4 shows a detail of the cesium

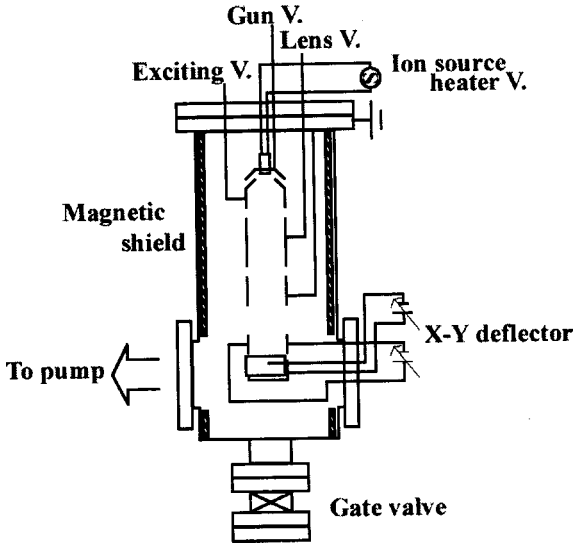

FIG. 3. Schematic drawing of the Li beam gun. This gun consists of an ion gun with a Li source, a Pierce extractor, and cylindrical lens.

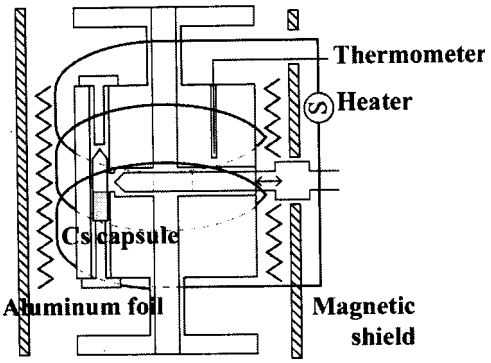

FIG. 4. Schematic drawing of the heat pipe-type cesium neutralizer.

neutralizer. The neutralizer is divided into a cesium cell part that stores cesium and a neutralizing cell part that is on the beam path. The neutralizer chamber is wound by a heater wire and is further covered by aluminum foil as thermal insulation. Its temperature is monitored by a thermocouple and kept at 180 °C during experiments because the ion beam is almost neutralized at about 180 °C (see Fig. 5). Cesium in a glass capsule mounted in the Cs cell part, and the glass capsule is broken by a moveable side bar and cesium is disclosed in the vacuum. This bar is also used as a shutter between the cesium cell and the neutralizing cell. It is opened for several seconds during the timing of plasma discharge. The neutralizer is also covered with a magnetic shield made by soft iron plates. The advantage of using cesium is that operation at low temperature is possible compared with lithium or sodium.

The beam energy is selected so that it offers both adequate spatial resolution and beam penetration. The spatial resolution is basically determined by the lifetime of the excised state of the Li atom. For the 15 keV beam the spatial resolution is less than $v_b \times \tau_{em} = 1.7$ cm and beam penetration is expected to be about 2×10^{18} m^{-2} of the line integrated density. For example, when plasma density is 10^{19} m^{-3}, the beam penetration depth is 0.2 m. The neutral beam diameter is about 20 mm in the CHS vacuum chamber, which is 2.5 m from the ion gun. A Faraday cup-type secondary emission detector is located just below the CHS vacuum chamber to monitor the neutral beam intensity. The neutral current is

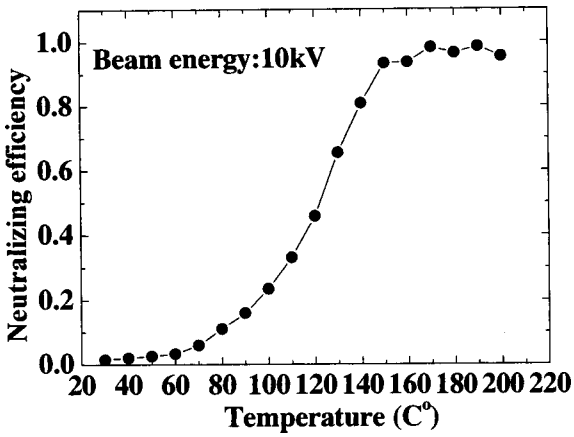

FIG. 5. Neutralizing efficiency as a function of the cesium oven temperature.

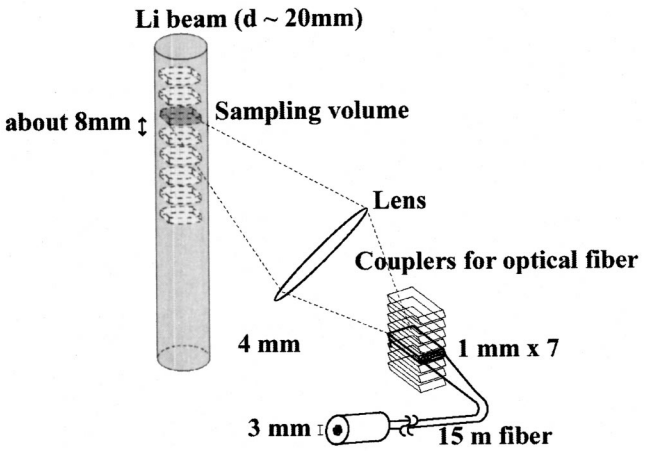

FIG. 6. Schematic drawing of the light collection optics.

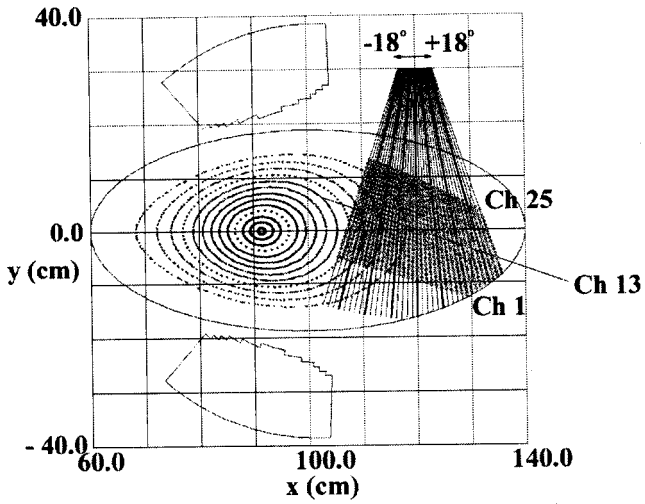

FIG. 7. The shadowed area is the measurable area on this system.

estimated from this secondary electron intensity assuming the secondary emission coefficient to be unity.

Light collection optics, which detect the light emission from the LiI resonance line, are located on the side port of the torus. The optical system consists of a lens, optical fibers, optical interference filters, and avalanche photodiode (APD) detectors. Figure 6 is a picture of the optical system. The light collection lens has a diameter of 100 mm, and a focal length $f=179.9$ mm. Twenty-five couplers for optical fibers are prepared on the light collection lens corresponding to 25 observation points along the beam. The coupler is numbered from No. 1 to No. 25 in an order from the top. The lithium beam is injected from the No. 25 observation point. In other words, No. 25 side observes outer side of the plasma and No. 1 observes inner side of the plasma. Distance from the coupler No. 13 (center channel of couplers) to a principal point of the light collection lens is 261.6 mm. The interval of the couplers is 4 mm. Spacing of the observation points are 8.8 to 9.6 mm depending on the location. Eight channel optical fibers can select eight observation points by using eight couplers among those. For each channel, seven fiber (diameter of 1 mm) are packed in a line at the coupler, and the image of the fiber cross section on the beam is roughly 2 mm $\times 14$ mm. The fibers are converted into a circle of 3 mm diameter and length of 15 m and introduced into the fiber box. The transmission efficiency is about 60% at 670.8 nm. The light is then made into a parallel ray by a plane-convex lens (diameter 30 mm, $f=60$ mm). The optical interference filter is mounted on this parallel ray region. Then, the light is converged onto the APD with a preamplifier whose frequency response is dc $\sim$100 kHz.

Since the angle between beam-line and sight-line is not a right angle, the observed emission suffers Doppler shift. A maximum Doppler shift at a beam energy of 15 keV is 0.9 nm in this system. The optical interference filters are selected with the center wavelength of 670.4 nm, bandwidth of 2 nm, and peak transmission of about 65%.

The injection beam line angle can be varied between +18° and −18° in the major radius direction. A two-dimensional profile is obtained by changing the beam injection angle shot by shot. A shaded area in Fig. 7 indicates the possible sample volume location determined by the 25 optical couplers. Beam-line at 0° injection angle and the sight-line crosses at the point $(x,y)=(1200\ \text{mm}, 0\ \text{mm})$.

Since the singal-to-noise (S/N) ratio for the present beam intensity is less than one $(S/N<1)$, the signals from APD detectors are introduced to phase sensitive detectors with 4 kHz beam modulation. The time constant of the phase sensitive detection is 3 ms in the present measurements.

V. EXPERIMENTAL RESULTS

Experiments have been carried out for the inboard limiter configuration, where the magnetic axis is at $R_{ax}=0.921$ m and the magnetic field strength is 0.95 T on the axis. Hydrogen plasmas are produced by electron cyclotron resonance heating with a gyrotron of 53 GHz and 170 kW. Neutral beam injection (NBI) heating is additionally applied using two beam lines (both in the codirection) with 40 keV and a total power of 1.3 MW. Electron cyclotron heating (ECH) is applied from $t=20$ to 120 ms and NBI from $t=80$ to 180 ms, where $t=0$ is the start of the data acquisition for diagnostic instruments. Plasma density is controlled by preprogrammed gas puff system. In the resent experiments, the average electron density in the ECH phase is about 1×10^{19} m^{-3}. The average electron density in the NBI phase depends on the heating schemes and is 4×10^{19} m^{-3} in the present experiment. The core electron density profile is measured with yttrium aluminum garnet laser Thomson scattering, showing flat and parabolic profiles in ECH and NBI plasmas, respectively.

The measurements are carried out on a shot by shot basis by changing the Li beam injection angle in the major radius direction. Observation areas for two different operations are shown in Fig. 8. Area A is near the LCFS and area B is outside of it. These measurements were performed on different days. Therefore, plasma parameters for the two cases may not necessarily be the same. Figure 9 shows an example of light emission from the LiI resonance line for channel 17 with a beam line injection angle of −14° (the observation point is indicated in Fig. 8). Since the signal level is almost constant both during the ECH and NBI phases, the emission

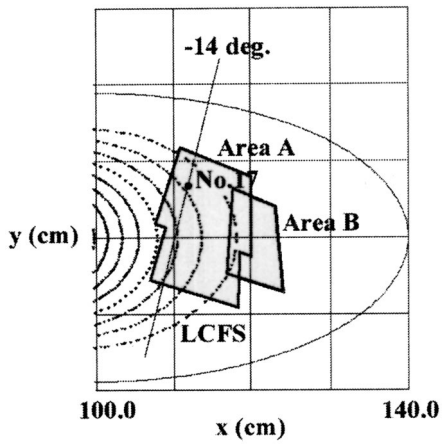

FIG. 8. The map of observation areas in the present experiments. The measurement is performed in areas A and B.

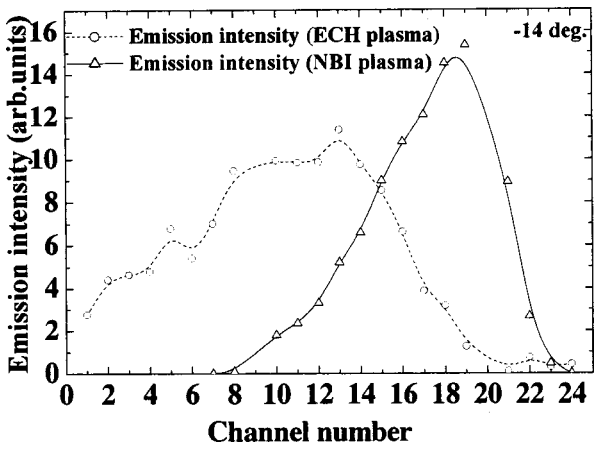

FIG. 10. Spatial distribution of the beam emission intensity for ECH and NBI plasma along the beam path with injection angle of −14°.

intensity averaged over 20 ms is used for 2D mapping shown later. It is noted that the remarkable increase of the emission intensity at the start of the NBI phase is primarily due to the increase of electron density near the LCFS. A signal from a killer puff, which is introduced to prevent high-energy electron production during the turnoff phase of the helical coils, is also detected at around $t=450$ ms. An expanded signal at this phase is also shown in the same figure. The emission signal comes from collisions with neutral hydrogen gas. Since the hydrogen gas distribution becomes uniform in a short period of time, the relative sensitivity between channels can be calibrated during the shot.

Figure 10 shows sample spatial distributions of the beam emission intensity for ECH and NBI plasmas along the injected beam path with an injection angle of −14°. The lithium beam is injected from the large channel number side. Those data were obtained from the three discharges with the same conditions, since our detector system has only eight channels at the moment. Beam attenuation is observed both in the ECH and NBI phases.

The electron density is reconstructed from these emission profiles. When the plasma density is large, the lithium beam is fully attenuated within the observation area. Then the density profile can be reconstructed using the beam attenuation method. For example, in the NBI discharge shown in Fig. 10, the emission intensity disappears completely near channel No. 7. An initial estimate of the zeroth-order density profile is first calculated using Eq. (11) . Then a more accurate density profile is calculated iteratively using Eq. (10) with effective rate coefficients given by the zeroth-order density profile.

When the emission profile is not measured completely within an observation range, the beam intensity method is used to reconstruct the electron density. In this method, gas calibration is necessary, in principle, to derive the value of sensitivity of the optical system as described in Sec. II B. However, since the density distribution was already calculated by the beam attenuation method for the NBI plasma in this experiment, this sensitivity calibration can be skipped. The proportional constant α in Eq. (12) can be determined experimentally from the data in the region of low density. Figure 11 shows the relation between the electron density and the beam emission intensity in the low density region.

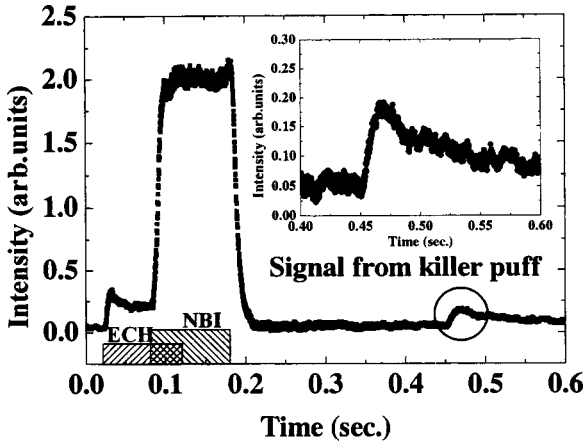

FIG. 9. An example of raw data of a light emission signal of the LiI resonance line taken at the Channel No. 17 with the beam injection angle of −14°. (See the beam line and the channel position shown as a dot in Fig. 8.) An inserted figure is an enlargement of the signal from the killer puff.

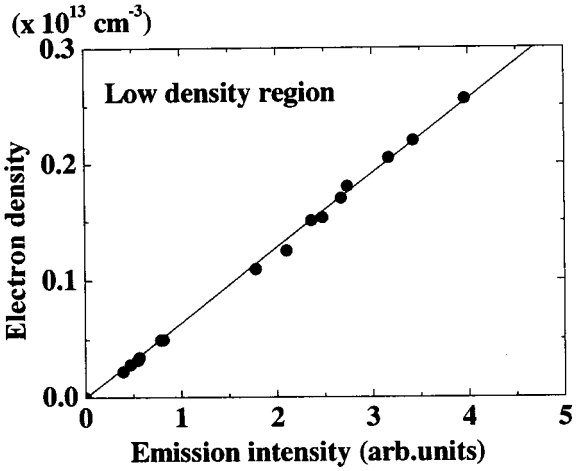

FIG. 11. Relation between emission intensity and election density at a low density region where beam attenuation is negligible. The electron density is obtained by the beam attenuation method.

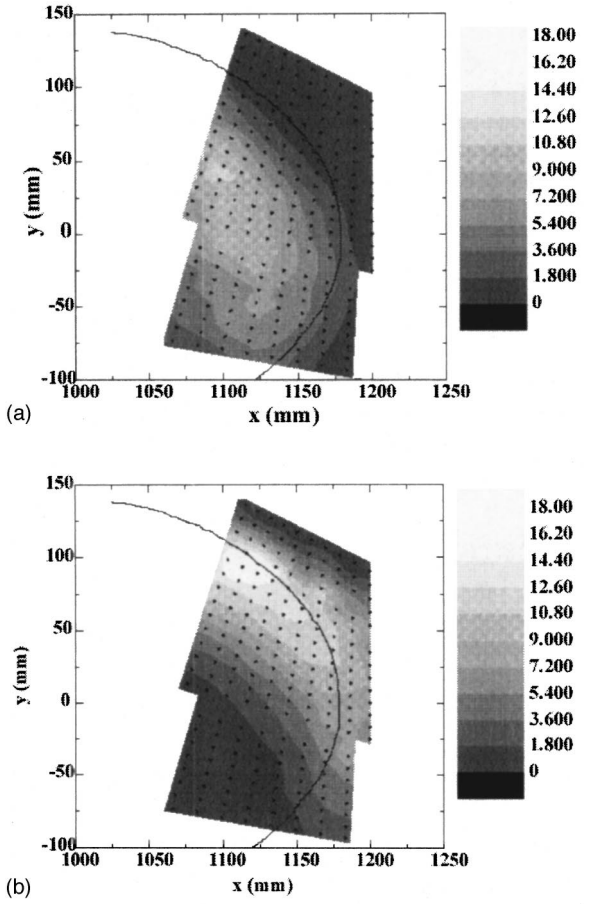

FIG. 12. Two-dimensional profiles of the beam emission intensity for (a) ECH plasma and (b) NBI plasma. (Observed in area A shown in Fig. 8.)

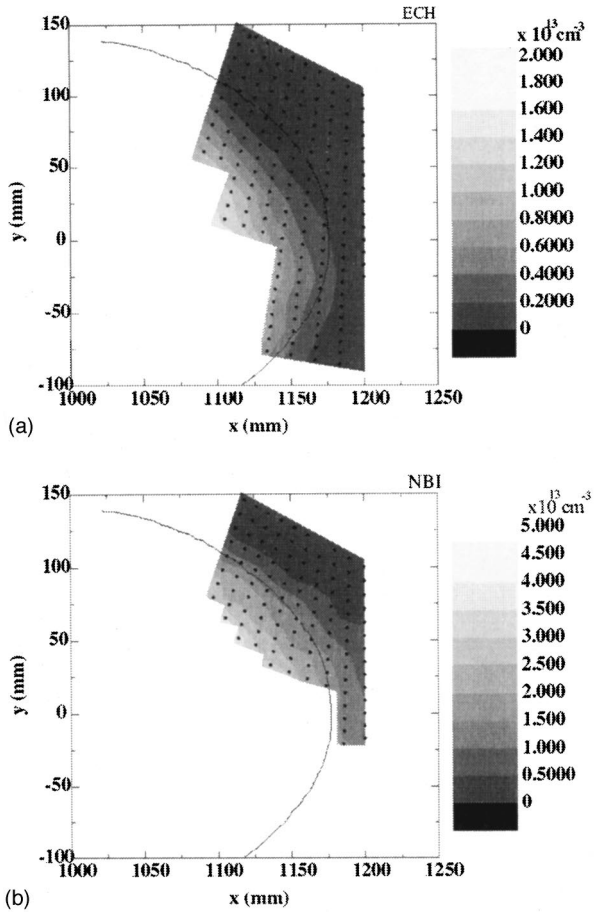

FIG. 13. Two-dimensional profiles of the electron density reconstructed from the data in Fig. 12 for (a) ECH plasma and (b) NBI plasma.

Data points in this figure are obtained from the data set for NBI plasma with beam injection angle from −18° to −12°.

The reconstructed density loses accuracy in the inner region of the plasma. This is because the reconstructed density profile is very sensitive to only a few percent experimental error as well as inaccuracy in the atomic data when the beam attenuation is severe. In this study, the adaptation rang in the beam attenuation method can be applied in the region from the edge to the position where the emission peaks. The beam intensity method can be applied for the plasma density up to 2×10^{19} m^{-3}, which is determined by comparison with the beam attenuation method.

Two-dimensional profiles of the beam emission intensity near the LCFS (area A) are shown in Fig. 12(a) for the ECH phase and Fig. 12(b) for the NBI. Smooth contour of the emission intensity along the LCFS are observed in the ECH phase. However, the contours are shifted down by roughly 2 cm. The contours deviate from the flux surfaces in the core region due to beam attenuation. The peak of the beam emission intensity roughly follows the LCFS in the NBI phase and rapidly decreases toward the core, suggesting a higher density plasma toward the LCFS. It is also noted that plasma is clearly observed outside the LCFS and that this plasma is spreading in the direction of the separatrix region. Two-dimensional profiles of the electron density, reconstructed from the data of Fig. 12 are shown in Fig. 13(a) for the ECH phase and Fig. 13(b) for the NBI plasma. In the ECH phase, plasma is distributed inside the LCFS. While, in the NBI phase, plasma is even distributed outside the LCFS.

Next, measurements are extended to the outer region (area B). A two-dimensional map of the beam emission intensity for the NBI phase is shown in Fig. 14, which was obtained in similar discharge conditions as before but on a different day. Figure 15 shows the two-dimensional electron density profile during the at NBI phase. It is again shown

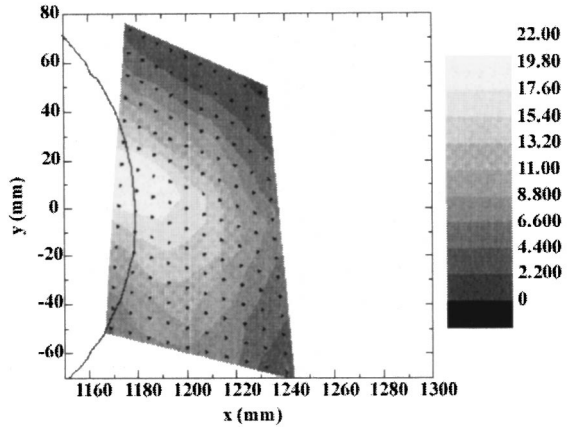

FIG. 14. Two-dimensional profile of the beam emission intensity outside of the LCFS in NBI phase. (Observed in area B shown in Fig. 8.)

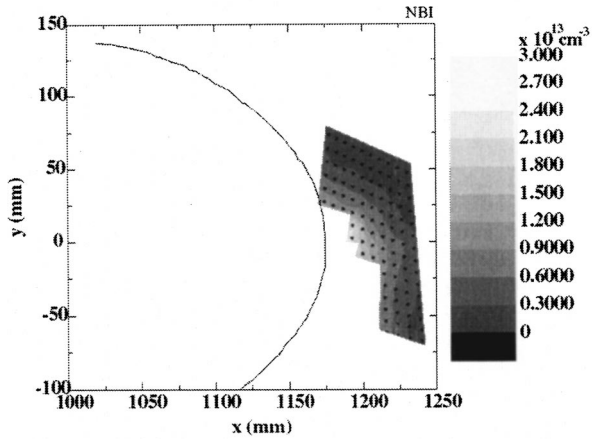

FIG. 15. Two-dimensional profile of the electron density reconstructed from the data in Fig. 14 for NBI plasma.

that plasma spreads outside the LCFS toward the separatrix region, consistent with the previous observation.

VI. DISCUSSION

In the previous section, several examples of two-dimensional electron density profile measurement in the edge and separatrix region of helical device CHS using the lithium neutral beam probe are introduced. This is the first demonstration of two-dimensional diagnostic of density profiles with the LiBP. There still remain several issues to be improved, which will be discussed below.

Relative sensitivities between channels are calibrated by detecting signals at the killer puff phase, where the LiI emission signals are caused by collisions with uniformly filled neutral hydrogen gas. This method alleviates the need for monitoring the absolute value or gradual change of the beam intensity during the day. Actually it is not easy to measure the beam intensity accurately in the presence of the magnetic field. On the other hand, because of a rather small signal level at the killer puff phase in the present experiments, the calibration data fluctuate by up to 10%. The resultant fluctuation of the relative sensitivities is the major source of error in the determination of the 2D beam emission profiles. Additional gas puffing near the LiBP port is being planned on order to improve the calibration accuracy.

The spatial resolution is determined by the effective lifetime of the lithium $2p$ state. When collisions are rare, it is determined roughly by $v_b \times \tau$ which is 1.7 cm for the 15 keV beam. This time of flight also affects the shift of the observation point. The observed shift of the emission profile contour near the LCFS in ECH phase by 2 cm is consistent with this estimate. On the contrary, in the higher density NBI phase, multiple processes become important due to more frequent collisions, making the effective lifetime shorter. Then the spatial resolution should be better and the shift of the emission profile should be less. This effect was estimated in detail by McCormick *et al.* using a collisional-radiative model for the atomic processes, and their result showed that the spatial resolution is 0.5 cm or less even for a higher energy beam of 30–70 keV.[11] Such calculation has not been done yet for our data, but it is reasonable to assume a similar shortening of the time of flight in NBI plasmas. The 2D electron density profiles shown here do not include the shift of the observation point due to the time of flight. The effect of this shift and its dependence on density should be considered for more detailed discussion.

On CHS, electron temperature becomes less than 10 eV outside of the LCFS for NBI plasmas.[12] For example, when the electron density is 1×10^{18} m^{-3}, the value of the emission rate coefficient for a 5 eV plasma becomes about 66% of the value for a 20 eV plasma. In the low electron temperature region, a detailed Te profile measurement is necessary which is not possible with LiBP only. Collaboration with other diagnostics is under discussion. Then density profile reconstruction will be improved.

The reconstructed electron density at the LCFS seems 1.5 times as large as that roughly estimated from the core density profile measured by the Thomson scattering and the line integrated density by the 2 mm interferometer. Effects such as the effective Z are under consideration, but a reasonable answer has not been found yet.

The experimental data suggests that the ECH plasma is confined inside the LCFS, since plasmas with density above 10^{18} m^{-3} do not exist outside of the LCFS. In contrast, the NBI plasma is spreading toward the separatrix region and noticeable amount of plasma is confined in this ergodic region in spite of the inboard limiter configuration. Plasma with density of 10^{19} m^{-3} even exists 4 cm beyond the LCFS along the equatorial plane. On the CHS, the field line length just outside the LCFS is about 3 m because the rotational transform $\iota/2\pi$ is almost unity at this area and there are four mirror structures. A part of plasma that escapes to outside LCFS is trapped in those mirrors. Therefore the plasma is not necessarily lost immediately, even though the magnetic configuration has an inboard limiter. Comparison of plasma structure in this region between the inbord limiter configuration and the magnetic limiter configuration is planned near future. These studies will be useful for actual design of the diverter in heliotron type devices.

Since the beam current is presently in the range of 0.05–0.1 mA with the 6 mm diameter ion source and the phase sensitive detection method is adopted, the time response is limited to 3 ms at the moment. Improvement of the signal-to-noise ratio is necessary to extend the time response by removing the phase sensitive detection. Actually, a 10 mA class lithium beam with a larger diameter β-eucriptite source has been developed by D. M. Thomas and is used for fluctuation study up to 100 kHz range.[9] The installation of a larger ion gun with movable beam injector is being planned to extend our diagnostic capabilities to study magnetohydrodynamics around the LCFS.

[1] K. Kadota, K. Tsuchida, Y. Kawasumi, and J. Fujita, Plasma Phys. **20**, 1011 (1978).
[2] H. Iguchi, K. Takagi, K. Takasugi, T. Shoji, M. Hosokawa, M. Fujiwara, and K. Ikegami, Rev. Sci. Instrum. **56**, 1056 (1985).
[3] K. McCormick and ASDEX team, Rev. Sci. Instrum. **56**, 1063 (1985).
[4] A. Pospieszyk, F. Aumayr, H. L. Bay, E. Hintz, P. Leismann, Y. T. Lie, G. G. Ross, D. Rusbuldt, R. P. Schweer, and H. Winter, J. Nucl. Mater. **128/129**, 574 (1989).
[5] S. Sasaki, S. Takamura, M. Ueda, H. Iguchi, J. Fujita, and K. Kadota, Rev. Sci. Instrum. **64**, 1699 (1993).

[6] S. Zoletnik, S. Fieldler, G. Kocsis, K. McCormick, J. Schweinzer, and H. P. Winter, Plasma Phys. Controlled Fusion **40**, 1399 (1998).
[7] M. Brix, A. Korotkov, M. Lehnen, P. Morgan, *et al.*, *Proceedings of the 28th EPS Conference on Controlled Fusion and Plasma Physics* 25A, 389 (2001).
[8] A. M. Howald, J. M. McChesney, and W. P. West, Rev. Sci. Instrum. **66**, 312 (1995).
[9] D. M. Thomas, Rev. Sci. Instrum. **66**, 806 (1995).
[10] T. Morisaki, A. Komori, O. Motojima, and LHD Experimental Group, Rev. Sci. Instrum. **74**, 1865 (2002).
[11] K. McCormick, S. Fiedler, G. Kocsis, J. Schweinzer, and S. Zoletnik, Fusion Eng. Des. **34–35**, 125 (1997).
[12] K. Ohkuni *et al.*, Phys. Plasmas **8**, 4035 (2001).